Quantitative Dynamic Thoracic MRI: Application to Thoracic Insufficiency Syndrome in Pediatric Patients

Yubing Tong, PhD • Jayaram K. Udupa, PhD • Joseph M. McDonough, MS • E. Paul Wileyto, PhD •
Anthony Capraro, MBS • Caiyun Wu, MS • Suzanne Ho, BA • Nirupa Galagedera, BA • Divya Talwar, MPH •
Oscar H. Mayer, MD • Drew A. Torigian, MD • Robert M. Campbell, MD

Background: Available methods to quantify regional dynamic thoracic function in thoracic insufficiency syndrome (TIS) are limited.

Purpose: To evaluate the use of quantitative dynamic MRI to depict changes in regional dynamic thoracic function before and after surgical correction of TIS.

Materials and Methods: Images from free-breathing dynamic MRI in pediatric patients with TIS (July 2009–August 2015) were retrospectively evaluated before and after surgical correction by using vertical expandable prosthetic titanium rib (VEPTR). Eleven volumetric parameters were derived from lung, chest wall, and diaphragm segmentations, and parameter changes before versus after operation were correlated with changes in clinical parameters. Paired analysis from Student *t* test on MRI parameters and clinical parameters was performed to detect if changes (from preoperative to postoperative condition) were statistically significant.

Results: Left and right lung volumes at end inspiration and end expiration increased substantially after operation in pediatric patients with thoracic insufficiency syndrome, especially right lung volume with 22.9% and 26.3% volume increase at end expiration (*P* = .001) and end inspiration (*P* = .002), respectively. The average lung tidal volumes increased after operation for TIS; there was a 43.8% and 55.3% increase for left lung tidal volume and right lung tidal volume (*P* < .001 for both), respectively. However, clinical parameters did not show significant changes from pre- to posttreatment states. Thoracic and lumbar Cobb angle were poor predictors of MRI tidal volumes (chest wall, diaphragm, and left and right separately), but assisted ventilation rating and forced vital capacity showed moderate correlations with tidal volumes (chest wall, diaphragm, and left and right separately).

Conclusion: Vertical expandable prosthetic titanium rib operation was associated with postoperative increases in all components of tidal volume (left and right chest wall and diaphragm, and left and right lung tidal volumes) measured at MRI. Clinical parameters did not demonstrate improvements in postoperative tidal volumes.

©RSNA, 2019

Online supplemental material is available for this article.

Thoracic insufficiency syndrome (TIS) (1) is a rare and serious childhood disorder involving thoracic volume depletion deformity, which affects fewer than 4000 children in the United States, and Jeune syndrome, which has an incidence of between one in 100 000 and one in 300 000 live births (2). Much of the morbidity in untreated TIS is because of progressive restrictive respiration, leading to respiratory failure and increased risk of early mortality (3). Surgical management of TIS can substantially limit respiratory decline (4). However, individual patients have variable but generally poor clinical outcomes because TIS is associated with heterogeneous group of neuromuscular, syndromic, structural, and idiopathic diagnoses that affect the chest wall and spine (4). Although 24% of children with TIS treated by using vertical expandable prosthetic titanium rib (VEPTR) have a subsequent improvement in respiratory assistance requirements, 64% remain stable and 12% continue to decline.

Thus, VEPTR generally prevents or slows deterioration rather than providing improvement in TIS (5).

Currently, the prime quantitative measures for corrective procedures have remained the anteroposterior and lateral radiographic Cobb angles (6–10), although these are essentially measurements of only the scoliotic disease. There is no useful correlation between Cobb angles and lung vital capacity before or after operation (11), which limits their health assessment value (12).

Radiography (6–10), CT (13–20), MRI (21–23), cine MRI (22), cine CT (24), and US (25) have been used to depict spinal and chest wall deformities. However, none of these methods conventionally define the dynamic loss of thoracic function as a ventilatory pump in TIS. Cine four-dimensional (4D) CT (26–28) can help to define thoracic motion but it has the disadvantage of radiation exposure, which for young children is problematic. Dynamic thoracic

Abbreviations

4D = four dimensional, LHTV = left hemidiaphragm tidal volume, LLTV = left lung tidal volume, LLVEE = left lung volume at end expiration, LLVEI = left lung volume at end inspiration, LTV = lung tidal volume, RHTV = right hemidiaphragm tidal volume, RLTV = right lung tidal volume, RLVEE = right lung volume at end expiration, RLVEI = right lung volume at end inspiration, TIS = thoracic insufficiency syndrome, VEPTR = vertical expandable prosthetic titanium rib

Summary

By using quantitative dynamic MRI, analysis of lung tidal volume in patients with thoracic insufficiency syndrome can assess postoperative effects on bilateral chest wall and diaphragm dynamics of breathing.

Key Points

- Quantitative dynamic thoracic MRI showed that left and right average lung volumes at end inspiration and end expiration increased substantially (eg, 23% and 26% increase for right lung volume at end expiration [$P = .001$] and end inspiration [$P = .002$], respectively) after operation in pediatric patients with thoracic insufficiency syndrome.
- Quantitative MRI also showed improvement in average lung tidal volumes (43.8% and 55.3% increase for left lung tidal volume and right lung tidal volume; $P < .001$) after operation for TIS, whereas conventional lung function testing showed no change.

MRI (29–31) is nonionizing and can be performed without breath holding or wearing devices for respiratory gating that is usually required by traditional cine MRI techniques (32). Quantitative dynamic thoracic MRI includes the advantage of free-breathing MRI acquisition, along with the synthesis of an optimized 4D cine respiratory cycle, and subsequent analysis of compartmental changes in lung volume that can be attributed to bilateral chest wall and diaphragm displacements. From these displacements, the overall mechanical function of the thorax as a ventilatory pump can be assessed with respect to pre- and postoperative structure of the spine, ribs, and implanted instrumentation.

Although pulmonary function testing (11,33) can infer bilateral thoracic function, it cannot provide regional data for individual lung, chest wall, and hemidiaphragm function. In this study, we performed quantitative dynamic MRI during tidal breathing. The purpose of this study was to use quantitative dynamic MRI to depict changes in dynamic function of the lungs and chest before and after surgical correction of TIS in pediatric patients by comparing left and right chest wall and hemidiaphragmatic components of tidal volumes before and after VEPTR treatment, and to analyze their relationships to pulmonary function tests and other clinical parameters. The central hypothesis for this study is that VEPTR treatment improves tidal ventilatory capacities of the chest wall and diaphragm in patients with TIS as manifested by improvement in quantitative dynamic MRI parameters after treatment.

Materials and Methods

Patients

This retrospective study was approved by the institutional review board at the Hospital of the University of Pennsylvania (Philadelphia, Pa) and was Health Insurance Portability and Accountability Act compliant. All patient data was previously acquired by using a prospective research protocol previously approved by the institutional review board at the Children's Hospital of Philadelphia (Pa) and the University of Pennsylvania. Consecutive patients with TIS over a 10-year period who received VEPTR and who underwent both pre- and posttreatment dynamic MRI at our TIS center were included in this analysis (Fig 1). Patients who underwent an operation before undergoing their first dynamic MRI or who underwent a previous thoracic operation were excluded. In total, 25 patients were finally selected according to the inclusion and exclusion criteria as shown in Figure 1.

Data Acquisition

Imaging.—Patient demographic information, anteroposterior and lateral radiographs, and dynamic MRI data preoperatively close to the date of initial operation and approximately 1.5 years postoperatively were included for analysis. For patients who were younger than 6 years, dynamic MRI was performed in tidal breathing during sedation with general anesthesia and ventilator support. For older patients (>6 years), dynamic MRI was performed by using free breathing (no anesthesia or ventilator support). The dynamic MRI protocol was as follows: 3.0-T imager (Siemens Healthcare, Erlangen, Germany), true-fast imaging with steady-state precession sequence; repetition time msec/echo time msec, 3.82/1.91; voxel size, approximately $1 \times 1 \times 6$ mm³; $320 \times 320 \times 38$ matrix; bandwidth, 558 Hz; flip angle, 76°; and one signal average. For each sagittal location in the thorax, section data were obtained during 8–14 tidal breathing cycles at approximately 200 msec per section; acquisition time was 10–20 minutes.

Clinical parameters.—Forced vital capacity, total lung capacity, thoracic and lumbar Cobb angles (thoracic Cobb angle measurement and lumbar Cobb angle measurement, respectively), respiratory rate, and assisted ventilation rating data were obtained from hospital medical records. We also recorded the resting pulse oximetry values before and after operation. The assisted ventilation rating (5) was previously developed as an outcome measure for a prospective multicenter clinical trial of the VEPTR device for treatment of TIS with scores defined as follows: +0, room air; +1, supplemental oxygen; +2, night ventilation; +3, part-time ventilation or continuous positive airway pressure; +4, full-time ventilation.

Image Processing and Analysis

The quantitative dynamic MRI method was performed as follows:
  1. 4D image construction. The number of two-dimensional free-breathing dynamic MRI sections acquired in a patient examination is typically 2000–3000, from which a small set of 175–320 sections (representing one 4D volume over one respiratory cycle) is selected by using an optimization method (32). The accuracy of this method in volume measurement is shown to be approximately 97% (32) by using a 4D dynamic phantom that used a three-dimensional printed model of the lungs of a healthy participant. Subsequently, MRI signal intensities
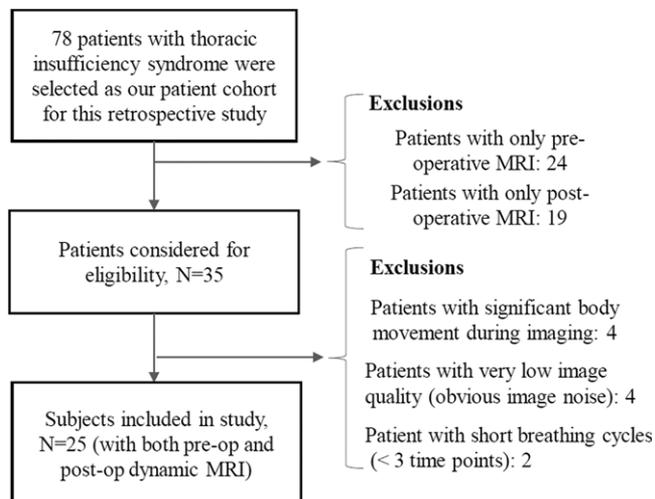
Figure 1: Patient inclusion and exclusion flowchart.

are standardized (34,35) to a standard intensity scale to facilitate MRI analysis, which will enable the voxel intensity values to have the numeric meaning for different tissues (ie, the same organs and tissues across all patients and participants should have similar intensities after intensity standardization).

2. Lung segmentation. Left and right lungs were separately segmented in 4D volume at end-inspiration and end-expiration phases by using the fuzzy connectedness engine (36) (Fig 2). The accuracy of lung segmentation by using this method was reported to have a true-positive volume fraction of 0.91 and a false-positive volume fraction of 0.03, with intra-and interoperator reproducibility of 94% and 90%, respectively (36).

3. Separation of chest wall and diaphragmatic components of lung excursion. By subtracting end-expiration images from end-inspiration images for each lung, we create lung excursion difference images. From these difference images, the chest wall and diaphragmatic components of lung excursion are separately derived (Fig 3). This process is performed independently for both left and right halves of the thorax.

4. Computation of volumes and tidal volumes. From the output of the previous two steps, we computed 11 volumetric parameters, as follows: Left lung volume at end inspiration (LLVEI), right lung volume at end inspiration (RLVEI), left lung volume at end expiration (LLVEE), right lung volume at end expiration (RLVEE), left lung tidal volume (LLTV), right lung tidal volume (RLTV), total lung tidal volume (LTV), left hemidiaphragm tidal volume (LHTV), right hemidiaphragm tidal volume (RHTV), left chest wall tidal volume, and right chest wall tidal volume), in which LLTV = LLVEI − LLVEE, RLTV = RLVEI − RLVEE, and LTV = LLTV + RLTV.

Clinical parameters were forced vital capacity, total lung capacity, resting breathing rate (respiratory rate), assisted ventilation rating, and signed thoracic and lumbar Cobb angles on the anteroposterior radiograph (thoracic Cobb angle measurement, lumbar Cobb angle measurement), on which a positive value meant that the respective spinal curve was convex to the right and a negative value meant that the respective spinal curve was convex to the left.

We compared changes of MRI parameters (lung volumes and component tidal volumes) with changes in clinical parameters from preoperative to postoperative imaging, and the associations between MRI and clinical parameters.

Statistical Analysis

Analysis was conducted by using software (Stata 15; Stata Corporation, College Station, Tex). Our goal was to determine whether there were statistically significant changes in MRI parameters (lung volumes and tidal volumes) from pre- to postoperative states with Bonferroni correction (37) for multiple comparisons, and P less than .05 was considered to indicate statistical significance. A secondary goal was to determine the association between MRI and clinical parameters and their changes before to after operation. Repeated measures were analyzed by using paired t tests (before vs after comparisons) and fitted by using generalized estimating equations, which account explicitly for the correlation of observations within the patient. Regressions included an indicator for pre- or posttreatment condition and time-varying adjustments for projected patient growth between pre- and posttreatment dates.

Results

Our cohort was composed of 13 male and 12 female patients (preoperative mean age, 5.1 years ± 4.2 [standard deviation]; and postoperative mean age, 6.7 years ± 4.2), with the following demographics: 18 white patients (17 non-Hispanic patients and one Hispanic or Latino patient), two African American patients (one non-Hispanic patient and one Hispanic patient), one Asian patient, and four patients who identified as other. The 25 patients were selected from 78 patients according to the inclusion and exclusion criteria as shown in Figure 1.

Qualitative Analysis of Radiographs and Three-dimensional Rendition Results of Lungs

Figure 4 shows images in a 7-year-old male patient with TIS and neuromuscular scoliosis who was treated with two VEPTR devices (left rib to pelvis and right rib to pelvis). The anteroposterior radiographs and three-dimensional renditions of the lungs at end inspiration and end expiration derived from pre- and posttreatment dynamic MRI are shown. The key pretreatment volumes were as follows: LLVEI, 172 mL; RLVEI, 260 mL; LLVEE, 160 mL; and RLVEE, 240 mL. The posttreatment volumes were as follows: LLVEI, 365 mL; RLVEI, 442 mL; LLVEE, 301 mL; and RLVEE, 387 mL. Chest wall and diaphragm tidal volumes before treatment were 44.939 mL and 24.439 mL, respectively, and after treatment were 73.038 mL and 67.852 mL, respectively. Posttreatment pulmonary tidal volumes increased by 186.6% (left), 51.3% (right), and 103.1% (combined). Although we present quantitative dynamic MRI volumes in whole units of milliliters, we note that the precision of quantitative dynamic MRI in measuring volumes is up to the volume of 1 voxel, which roughly translates to three decimals in units of milliliter.

We created an animation to depict lung dynamics for this patient via three-dimensional renditions of their lungs from pre- and posttreatment data to illustrate the extent of improvement achieved by operation (Movies 1, 2 [online]). The animation depicts the changes in lung dynamics after operation in the

individual lungs and in their motion relationships, which cannot be viewed at two-dimensional dynamic displays of the individual sections of the constructed 4D volume. From the animation, we (ie, surgeons, pulmonologists, and radiologists) observed that the dynamic excursions of the lungs markedly increased postoperatively. More interestingly, the motions of the left and right lungs were asynchronous before operation, and postoperatively appeared more normally synchronous. This information is a unique feature of this method.

Quantitative Analysis on Tidal Volumes

Tables 1 and 2 summarize key statistics related to, respectively, MRI and clinical parameters for our cohort. All quantitative dynamic MRI volume parameters increased after operation, with an increase of 14.7%, 26.3%, 12.1%, and 22.9% for the average lung volumes of LLVEI, RLVEI, LLVEE, and RLVEE, respectively. Percent tidal volume increase for different components was even higher: LTV by 50.6% (43.8% for LLTV and 55.3% for RLTV); 33.3% for left chest wall tidal volume and 35.7% for right chest wall tidal volume; and 61.4% for LHTV and 72.1% for RHTV. Notably, increase in diaphragm tidal volume after operation was nearly twice that of the chest wall. Considering multiple comparisons, P values with Bonferroni correction are shown in Table 1. RLVEE and RLVEI showed significant increase after TIS operation ($P = .001$ and .002, respectively), and all P values were less than .001 for LLTV, RLTV, LHTV, RHTV, and left and right chest wall tidal volumes.

Both Cobb angles, thoracic Cobb angle measurement and lumbar Cobb angle measurement, decreased after operation with a mean reduction of 20.3% and 18.5%, respectively, implying that the thoracic and lumbar spine typically have less visible scoliotic curvature on the anteroposterior radiograph after surgical treatment. However, the clinical parameters forced vital capacity, total lung capacity, lumbar Cobb angle measurement, respiratory rate, resting pulse oximetry, and assisted ventilation rating did not show a statistically significant change from pretreatment to posttreatment states (Table 2).

Table 3 summarizes statistics related to the pre- to posttreatment change in tidal volumes. We used random-effects models (generalized estimating equation) to analyze the changes from preoperative to postoperative in tidal volumes. We adjusted for predicted tidal volume (from age) to account
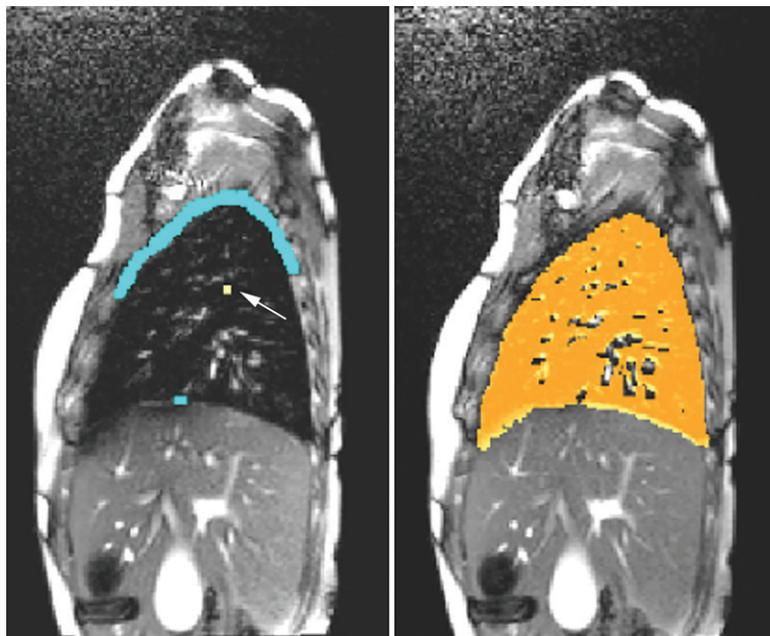

Figure 2: Illustration of seed specification for object and background tissues to perform lung segmentation. Sagittal section corresponding to end-expiration phase of four-dimensional dynamic MRI in a patient with thoracic insufficiency syndrome (left). Seeds for object (arrow) and background region (blue) are shown. Sagittal section with segmented right lung as color overlay (right).
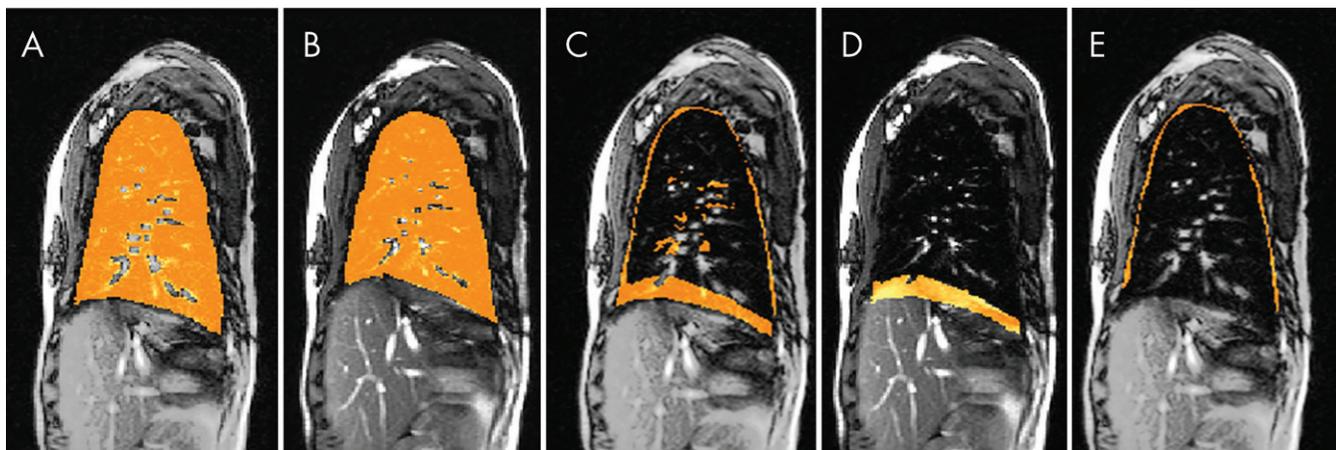

Figure 3: Illustration of delineation of excursion space from end inspiration to end expiration on four-dimensional constructed images at sagittal plane in a 12-year-old postoperative female patient . *A,* One representative sagittal section through the right lung at end inspiration with segmented right lung overlaid in orange. *B,* One representative sagittal section through the right lung at end expiration with segmented right lung overlaid in orange. *C,* Segmentation in *A* minus segmentation in *B* overlaid in orange on the MRI section on *B. D,* The MRI section shown in *B* with diaphragmatic component of excursion overlaid in orange. *E,* The MRI section shown in *B* with the chest wall component of excursion overlaid in orange.
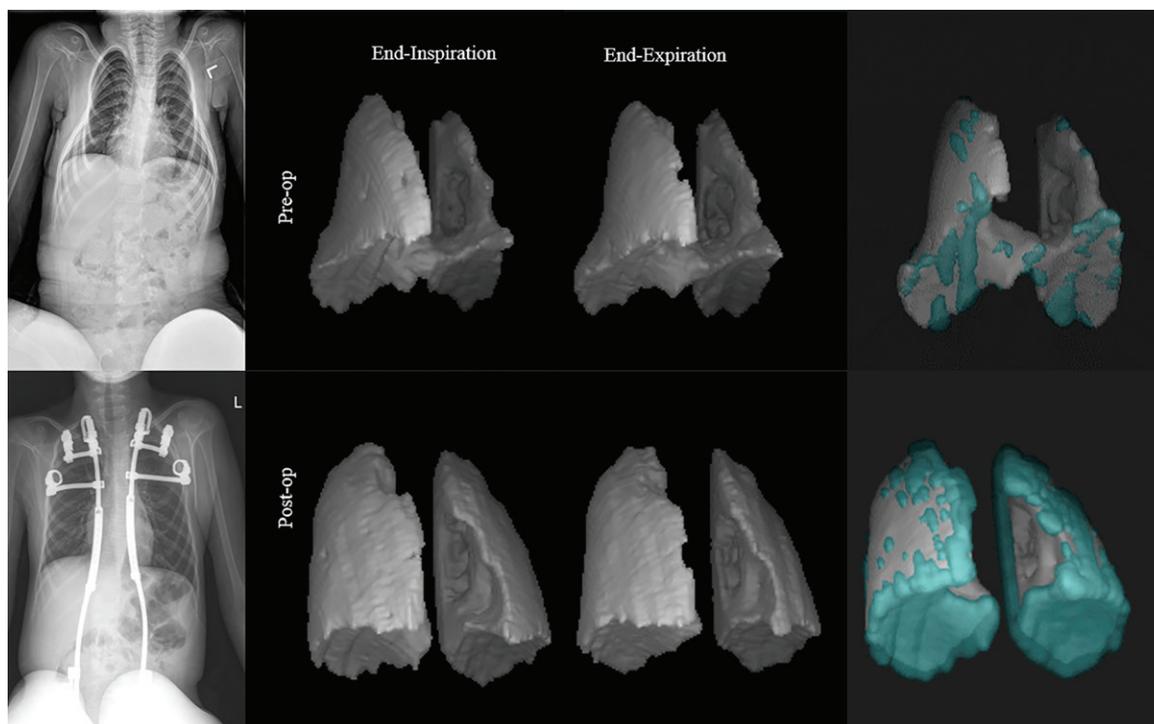
Figure 4: Radiographs (left) and three-dimensional renditions of the lungs in a 7-year-old male patient with thoracic insufficiency syndrome with neuromuscular scoliosis (spinal muscular atrophy II) are shown. Combined three-dimensional renderings (right) show the lungs at end inspiration (turquoise) and end expiration (gray).

Table 1: Descriptive Statistics of the Study Cohort before and after Operation for Thoracic Insufficiency Syndrome

Parameter	Preoperative TIS	Postoperative TIS	Average Increase in Volume (%)	P Value
Age (y)	5.1 ± 4.2	6.7 ± 4.2	…	.18
Height (cm)	94.5 ± 27.2	105.7 ± 27.2	…	.12
Weight (kg)	17.5 ± 10.2	20.2 ± 9.99	…	.21
Left lung volume at end inspiration (mL)	299 ± 260	343 ± 222	14.7	.03
Right lung volume at end inspiration (mL)	316 ± 263	399 ± 243	26.3	.002
Left lung volume at end expiration (mL)	199 ± 154	223 ± 134	12.1	.044
Right lung volume at end expiration (mL)	205 ± 159	252 ± 150	22.9	.001
Left lung tidal volume left lung tidal volume (mL)	32 ± 17	46 ± 23	43.8	<.001
Right lung tidal volume (mL)	47 ± 25	73 ± 33	55.3	<.001
Lung tidal volume (mL)	79 ± 37	119 ± 53	50.6	<.001
Left hemidiaphragm tidal volume (mL)	11 ± 6	18 ± 11	63.6	.002
Right hemidiaphragm tidal volume (mL)	21 ± 12	37 ± 20	76.2	<.001
Left chest wall tidal volume (mL)	21 ± 11	28 ± 13	33.3	<.001
Right chest wall tidal volume (mL)	28 ± 14	38 ± 15	35.7	<.001

Note.—Data are mean ± standard deviation. There were 13 male patients and 12 female patients. To calculate the average increase in volume, the following equation was used: [(postoperative − preoperative)/preoperative] × 100. There were 15 patients with neuromuscular disease, seven patients with congenital disease, one patient with idiopathic disease, one patient with syndromic disease, and one patient with other type of disease. All volumes are in milliliters. Bonferroni correction was performed for multiple comparisons (Bonferroni correction calculation: .05/11 = .005). TIS = thoracic insufficiency syndrome.

for potential patient growth between the pre- and postoperative examinations. In Table 3, all tidal volume parameters significantly increased after operation with z scores roughly between 2 and 3 and medium to large effect size. RLTV and RHTV particularly stand out by showing the largest change compared with other components.

Regressions were adjusted for child growth predicted from age because of pre- and posttreatment age differences of the same patient. Associations between MRI parameters (independent) and clinical parameters (dependent) that were statistically significant or that showed borderline significance are shown in Table 4. For example, right chest wall tidal volume as an independent

Table 2: Clinical Parameters of the Patient Cohort before and after Operation for Thoracic Insufficiency Syndrome

Parameter	Mean Preoperative TIS	Mean Postoperative TIS	Average Increase in Measurement (%)	P Value
Forced vital capacity (mL)	1050 (506, 1593)	968 (524, 1413)	−7.8	.80
Total lung capacity (mL)	1421 (408, 2433)	1790 (1271, 2308)	26.0	.42
Respiratory rate (cycle/min)	29.9 (25.8, 34.0)	25.3 (22.33, 28.30)	−15.4	.07
Assisted ventilation rating	1.4 (0.3, 2.5)	0.7 (0.1, 1.4)	−50.0	.23
Thoracic Cobb angle measurement (degree)	56 (35, 60)	44 (40, 67)	−21.4	.53
Lumbar Cobb angle measurement (degree)	26 (14, 46)	22 (6, 30)	−15.4	.24
Resting pulse oximetry	96.7 (96.5, 98.9)	98.0 (97.2, 98.8)	1.3	.60

Note.—Data in parentheses are 95% confidence intervals. To calculate the average increase in volume, the following equation was used: [(postoperative − preoperative)/preoperative] × 100. Bonferroni correction is used to account for multiple comparisons. These outcomes are uncorrelated (Bonferroni correction calculation: .05/7 = .007).

parameter will predict the outcome of assisted ventilation rating as a dependent parameter with effect size of 1.18 ($P < .001$).

Because clinical parameters did not show any statistically significant changes between the pre- and postoperative conditions, we tested the ability of the clinical parameters to predict MRI parameters, particularly tidal volumes. Cobb angles did not predict most of the tidal volumes except for lumbar Cobb angle measurement which showed strong association with LHTV with large effect size ($P = .003$). Other clinical parameters varied in their ability to predict tidal volumes. Respiratory rate was relatively unrelated to any tidal volume and hence not listed in the table. The average effect size for regression coefficients was approximately 0.5 for assisted ventilation rating and 0.4 for forced vital capacity (medium effects).

Discussion

Available methods to quantify regional dynamic thoracic function in patients with thoracic insufficiency syndrome (TIS) are limited. In our study, we developed the quantitative dynamic MRI method to fill the void that currently exists for practical assessment of regional dynamic thoracic function in TIS. Our larger goal is to develop a scientific basis to objectively assess the therapeutic effects of vertical expandable prosthetic titanium rib (VEPTR) and other outcomes for patients with this disease, and to improve the optimization of treatment techniques that are implemented. We show that VEPTR operation facilitates substantial postoperative improvement in regional thoracic dynamics on the basis of assessments at quantitative dynamic MRI because all components of tidal volume increased after the operation. Left and right lung volumes at end inspiration and end expiration increased substantially (12%–26.2%) after operation ($P < .05$; 95% confidence interval: −8.2, 31.5). Increases in tidal volumes after operation were substantial (33.5%–72.1%), and the right lung and right hemidiaphragm exhibited the largest changes (54.9% and 72.1%, respectively).

By proposing these new metrics, we show their association with currently used clinical metrics, which are incapable of measuring the local-regional changes found by using quantitative dynamic MRI. Lung ventilation dynamics are complex, especially when the thoracic ventilatory apparatus is distorted because of deformities in the skeleton and, as we observed, paradoxic motions of thoracic

component structures may occur. Information about these motions is completely lost, and misleading interpretations may occur when only global thoracic function or spinal curvature is measured to understand these underlying phenomena.

The passive components of volume can be parsed out by using MRI (eg, LLVEI and RLVEI), and different components of tidal volumes can be measured that have not been addressed in previous work. We observed that chest wall tidal volume was generally larger than the diaphragmatic component, although the pre- to postoperative change in tidal volume was greater for the diaphragm than the chest wall component. Although all tidal volumes increased after operation, interestingly, the increase in tidal volumes of the right lung components (right chest wall tidal volume and RHTV) was substantially greater than that of other components. This suggests that restoration of the diaphragmatic excursion of the right hemithorax may be more important than that of the left hemithorax irrespective of the nature of the deformity. This could be because the right lung is larger overall, or there could be an underlying anatomic basis or TIS-related process that causes the right lung components to achieve a better gain in dynamics after VEPTR treatment. In our study group, 14 patients had substantial unilateral deformity (right side in nine patients and left side in five patients). This may be part of the reason for substantially higher gains in right chest wall tidal volume, RHTV, and RLTV compared with the left counterparts. However, we observed that in patients with right-sided deformity both RLTV and LLTV increased after treatment and that the increase in RLTV was significantly greater than that of LLTV (mean increases in RLTV and LLTV were 34.7 mL and 16.7 mL, respectively; $P < .05$). We did not observe a similar behavior in patients with left-sided deformity (changes in RLTV and LLTV were close and not statistically different; $P = .7$). Interestingly, for the remaining 10 patients with deformities that were mostly symmetric, increases in RLTV were also significantly greater than that in LLTV ($P = .01$), which possibly suggests that restoration of dynamics of the right lung is perhaps more important than restoring left lung dynamics, irrespective of the nature of the deformity. A curious phenomenon is revealed in the animation included in the multimedia material of this study (Movies 1, 2 [online]). There appears

Table 3: Relationship of Preoperative Tidal Volumes to Postoperative Tidal Volumes

Parameter	Tidal Volume Change (mL)	z Score	Effect Size	P Value
Left chest wall tidal volume	3.9 (0.3, 7.5)	2.2	0.5	.003
Left hemidiaphragm tidal volume	4.7 (0.3, 9.2)	2.1	0.5	.03
Right chest wall tidal volume	7.6 (2.2, 13.0)	2.8	0.6	.004
Right hemidiaphragm tidal volume	11.9 (4.3, 19.7)	3.0	0.7	.003
Left lung tidal volume	8.5 (1.6, 15.6)	2.4	0.5	.02
Right lung tidal volume	19.9 (7.6, 32.1)	3.3	0.7	.001

Note.—Data in parentheses are 95% confidence intervals. Data were adjusted for predicted title volume on the basis of age. To determine tidal volume change, the following equation was used: postoperative tidal volume (mL) − preoperative tidal volume (mL). Cohen (d) effect size for mean difference is defined as the difference of two population means divided by the standard deviation estimated from pooled data. Bonferroni correction is used to account for multiple comparisons. Bonferroni correction with P value of .05/6 = .008. Outcomes are correlated (r = 0.77). Bonferroni adjusted for correlation − 0.033.

Table 4: Associations of Quantitative Dynamic MRI Parameters with Clinical Measures by Using a Multivariable Model

Parameter	Regression Coefficient	z Score	Effect Size	P Value
Left hemidiaphragm tidal volumes versus lumbar Cobb angle (n = 19)	0.14 (−0.02, 0.21)	3.0	0.89	.003
Right hemidiaphragm tidal volumes versus lumbar Cobb angle (n = 19)	−0.12 (−0.39, 0.17)	−1.9	0.56	.06
Left hemidiaphragm tidal volumes versus thoracic Cobb angle (n = 19)	−0.08 (−0.18, 0.02)	−1.8	0.42	.07
Right hemidiaphragm tidal volumes versus thoracic Cobb angle (n = 19)	0.11 (−0.09, 0.22)	1.9	0.44	.06
Left hemidiaphragm tidal volumes versus maximum* (n = 19)	0.11 (−0.17, −0.01)	1.9	0.44	.06
Left lung tidal volumes. assisted ventilation rating (n = 17)	8.2 (−0.01, 0.02)	3.5	0.86	<.001
Right chest wall tidal volumes versus assisted ventilation rating (n = 17)	5.5 (−0.03, 0.10)	4.9	1.2	<.001
Right lung tidal volumes versus assisted ventilation rating (n = 17)	7.9 (−0.02, 0.04)	3.6	0.87	<.001
Right hemidiaphragm tidal volume versus forced vital capacity (n = 8)	0.16 (−1.53, 0.73)	2.5	0.88	.01
Right lung tidal volumes versus forced vital capacity (n = 8)	0.20 (−1.66, 0.72)	2.2	0.78	.03

Note.—Data in parentheses are 95% confidence intervals. Only statistically significant and borderline significant associations are listed. Regressions were adjusted for potential child growth predicted from age because of pre- and posttreatment age differences in the same patient. The correlation value to adjust Bonferroni is 0.75, with the operation of lowering the P value from .05 to .029; z score for one-sided testing, ≥1.89; z score for two-sided testing, ≥2.18.
* Refers to the larger of the thoracic Cobb angle and lumbar Cobb angle measurements.

to be asynchrony in the motion between left and right lungs before operation in a representative patient with TIS, which was corrected after operation, which showed that quantitative dynamic MRI can depict abnormalities that were previously inaccessible.

Although changes in Cobb angle after treatment of scoliosis have been studied extensively (5–15), their relationships to tidal volumes to our knowledge have not been examined. In this study, we found only one significant association for Cobb angle, namely lumbar Cobb angle measurement with LHTV. Overall, Cobb angle was incapable of predicting tidal volumes. However, assisted ventilation rating and forced vital capacity showed moderate ability in predicting tidal volumes.

Our study had limitations. The main limitation of this study was that the sample size was small. The small size did not permit us to perform analysis on the basis of TIS subtypes. We

understand that a larger sample size would increase study power, and we are continuing our research with more patients with TIS. Yet, in spite of population heterogeneity, our study has shown that quantitative dynamic MRI is able to depict the beneficial effects of treatment for regional thoracic function in TIS that clinical parameters were unable to show, and to our knowledge this is the first study to describe the use of dynamic MRI in the setting of TIS. The main current bottleneck in the quantitative dynamic MRI approach is lung segmentation, which requires interaction at the individual section level. We are looking into methods of improving the efficiency of this step by using machine learning.

In conclusion, in a small group of patients with thoracic insufficiency syndrome who were studied by using quantitative dynamic MRI of the thorax, the use of vertical expandable prosthetic titanium rib operation facilitated substantial improvement in thoracic dynamics. This was evidenced by postoperative

increases in all components of tidal volume. Restoration of the diaphragmatic excursion of the right hemithorax may be more important than that of the left hemithorax regardless of the nature of the deformity. Clinical parameters are unable to predict postoperative regional tidal volume improvements because of their lack of local-regional functional assessment of chest wall and diaphragmatic motion.

References

1. Campbell RM Jr, Smith MD. Thoracic insufficiency syndrome and exotic scoliosis. J Bone Joint Surg Am 2007;89(Suppl 1):108–122.
2. Mayer O, Campbell R, Cahill P, Redding G. Thoracic Insufficiency Syndrome. Curr Probl Pediatr Adolesc Health Care 2016;46(3):72–97.
3. Corona J, Matsumoto H, Roye DP, Vitale MG. Measuring quality of life in children with early onset scoliosis: development and initial validation of the early onset scoliosis questionnaire. J Pediatr Orthop 2011;31(2):180–185.
4. O'Brien A, Roth MK, Athreya H, et al. Management of Thoracic Insufficiency Syndrome in Patients With Jeune Syndrome Using the 70 mm Radius Vertical Expandable Prosthetic Titanium Rib. J Pediatr Orthop 2015;35(8):783–797.
5. Nossov SB, Curatolo E, Campbell RM, et al. VEPTR: Are We Reducing Respiratory Assistance Requirements? J Pediatr Orthop 2019;39(1):28–32.
6. Sankar WN, Albrektson J, Lerman L, Tolo VT, Skaggs DL. Scoliosis in-brace curve correction and patient preference of CAD/CAM versus plaster molded TLSOs. J Child Orthop 2007;1(6):345–349.
7. Segev E, Hemo Y, Wientroub S, et al. Intra- and interobserver reliability analysis of digital radiographic measurements for pediatric orthopedic parameters using a novel PACS integrated computer software program. J Child Orthop 2010;4(4):331–341.
8. Olgun ZD, Ahmadiadli H, Alanay A, Yazici M. Vertebral body growth during growing rod instrumentation: growth preservation or stimulation? J Pediatr Orthop 2012;32(2):184–189.
9. Glotzbecker MP, Gold M, Puder M, Hresko MT. Scoliosis after chest wall resection. J Child Orthop 2013;7(4):301–307.
10. Gantner AS, Braunschweig L, Tsaknakis K, Lorenz HM, Hell AK. Spinal deformity changes in children with long-term vertical expandable prosthetic titanium rib treatment. Spine J 2018;18(4):567–574.
11. Mayer OH, Redding G. Early changes in pulmonary function after vertical expandable prosthetic titanium rib insertion in children with thoracic insufficiency syndrome. J Pediatr Orthop 2009;29(1):35–38.
12. Goldberg CJ, Gillic I, Connaughton O, et al. Respiratory function and cosmesis at maturity in infantile-onset scoliosis. Spine 2003;28(20):2397–2406.
13. Alanay A, Hicazi A, Acaroglu E, et al. Reliability and necessity of dynamic computerized tomography in diagnosis of atlantoaxial rotatory subluxation. J Pediatr Orthop 2002;22(10):763–765.
14. Kotwicki T, Napiontek M. Intravertebral deformation in idiopathic scoliosis: a transverse plane computer tomographic study. J Pediatr Orthop 2008;28(2):225–229.
15. Hong JY, Suh SW, Park HJ, Kim YH, Park JH, Park SY. Correlations of adolescent idiopathic scoliosis and pectus excavatum. J Pediatr Orthop 2011;31(8):870–874.
16. Izatt MT, Adam CJ, Verzin EJ, Labrom RD, Askin GN. CT and radiographic analysis of sagittal profile changes following thoracoscopic anterior scoliosis surgery. Scoliosis 2012;7(1):15.
17. Doi T, Kido S, Kuwashima U, et al. A new method for measuring torsional deformity in scoliosis. Scoliosis 2011;6(1):7.
18. Gollogly S, Smith JT, Campbell RM. Determining lung volume with three-dimensional reconstructions of CT scan data: A pilot study to evaluate the effects of expansion thoracoplasty on children with severe spinal deformities. J Pediatr Orthop 2004;24(3):323–328.
19. Adam CJ, Cargill SC, Askin GN. Computed tomographic-based volumetric reconstruction of the pulmonary system in scoliosis: trends in lung volume and lung volume asymmetry with spinal curve severity. J Pediatr Orthop 2007;27(6):677–681.
20. Abul-Kasim K, Karlsson MK, Hasserius R, Ohlin A. Measurement of vertebral rotation in adolescent idiopathic scoliosis with low-dose CT in prone position - method description and reliability analysis. Scoliosis 2010;5:4.
21. Chu WCW, Li AM, Ng BKW, et al. Dynamic magnetic resonance imaging in assessing lung volumes, chest wall, and diaphragm motions in adolescent idiopathic scoliosis versus normal controls. Spine 2006;31(19):2243–2249.
22. Kotani T, Minami S, Takahashi K, et al. An analysis of chest wall and diaphragm motions in patients with idiopathic scoliosis using dynamic breathing MRI. Spine 2004;29(3):298–302.
23. Chu WCW, Ng BKW, Li AM, Lam TP, Lam WWM, Cheng JCY. Dynamic magnetic resonance imaging in assessing lung function in adolescent idiopathic scoliosis: a pilot study of comparison before and after posterior spinal fusion. J Orthop Surg Res 2007;2(1):20.
24. Yang D, Lu W, Low DA, Deasy JO, Hope AJ, El Naqa I. 4D-CT motion estimation using deformable image registration and 5D respiratory motion modeling. Med Phys 2008;35(10):4577–4590.
25. Chen W, Lou EH, Zhang PQ, Le LH, Hill D. Reliability of assessing the coronal curvature of children with scoliosis by using ultrasound images. J Child Orthop 2013;7(6):521–529.
26. Nehmeh SA, Erdi YE, Pan T, et al. Four-dimensional (4D) PET/CT imaging of the thorax. Med Phys 2004;31(12):3179–3186.
27. Keall PJ, Vedam SS, George R, Williamson JF. Respiratory regularity gated 4D CT acquisition: concepts and proof of principle. Australas Phys Eng Sci Med 2007;30(3):211–220.
28. Low DA, Nystrom M, Kalinin E, et al. A method for the reconstruction of four-dimensional synchronized CT scans acquired during free breathing. Med Phys 2003;30(6):1254–1263.
29. Wachinger C, Yigitsoy M, Rijkhorst EJ, Navab N. Manifold learning for image-based breathing gating in ultrasound and MRI. Med Image Anal 2012;16(4):806–818.
30. Cai J, Chang Z, Wang Z, Paul Segars W, Yin FF. Four-dimensional magnetic resonance imaging (4D-MRI) using image-based respiratory surrogate: a feasibility study. Med Phys 2011;38(12):6384–6394.
31. Wagshul ME, Sin S, Lipton ML, Shifteh K, Arens R. Novel retrospective, respiratory-gating method enables 3D, high resolution, dynamic imaging of the upper airway during tidal breathing. Magn Reson Med 2013;70(6):1580–1590.
32. Tong Y, Udupa JK, Ciesielski KC, et al. Retrospective 4D MR image construction from free-breathing slice Acquisitions: A novel graph-based approach. Med Image Anal 2017;35:345–359.
33. Motoyama EK, Deeney VF, Fine GF, et al. Effects on lung function of multiple expansion thoracoplasty in children with thoracic insufficiency syndrome: a longitudinal study. Spine 2006;31(3):284–290.
34. Zhuge Y, Udupa JK, Liu J, Saha PK. Image background inhomogeneity correction in MRI via intensity standardization. Comput Med Imaging Graph 2009;33(1):7–16.
35. Nyúl LG, Udupa JK. On standardizing the MR image intensity scale. Magn Reson Med 1999;42(6):1072–1081.
36. Tong Y, Udupa JK, Odhner D, et al. Interactive iterative relative fuzzy connectedness lung segmentation on thoracic 4D dynamic MR images. Proc SPIE Int Soc Opt Eng 2017;10137.
37. Sankoh AJ, Huque MF, Dubey SD. Some comments on frequently used multiple endpoint adjustment methods in clinical trials. Stat Med 1997;16(22):2529–2542.